

# We are IntechOpen, the world's leading publisher of Open Access books Built by scientists, for scientists

4,800

Open access books available

122,000

International authors and editors

135M

Downloads

Our authors are among the

154

Countries delivered to

TOP 1%

most cited scientists

12.2%

Contributors from top 500 universities



WEB OF SCIENCE™

Selection of our books indexed in the Book Citation Index  
in Web of Science™ Core Collection (BKCI)

Interested in publishing with us?  
Contact [book.department@intechopen.com](mailto:book.department@intechopen.com)

Numbers displayed above are based on latest data collected.  
For more information visit [www.intechopen.com](http://www.intechopen.com)



# Poisson's Ratio and Mechanical Nonlinearity Under Tensile Deformation in Crystalline Polymers

Koh-hei Nitta and Masahiro Yamana

*Division of Material Sciences, Graduate School of Natural Science and Technology,  
Kanazawa University, Kakuma, Kanazawa,  
Japan*

## 1. Introduction

Semicrystalline polymers contain liquid-like amorphous and ordered crystalline phases. When solidified from the pure melt, these polymers show a spherulitic structure in which crystalline lamellae composed of folded chain crystallites radiate from the center of the spherulite in such a way that a constant long period or crystallinity is approximately maintained. The amorphous regions reside in the interlamellar regions in the form of tie chains, whose ends are attached to adjacent lamellae; loop chains, whose ends are attached to the same lamella; cilia chains with only one end attached to a lamella (or dangling chain ends), and floating chains which are not attached to any lamellae. This hierarchical structure is illustrated in Figure 1.

Nitta-Takayanagi have introduced the idea of stacked lamellae running parallel forming clusters, the sizes of which are in the range of the end-to-end distance of single Gaussian chains, to explain the tensile yielding and necking phenomena (Nitta & Takayanagi, 2003). Similar concepts to the lamellar cluster have been proposed by other investigators. Based on transmission electron microscopy (TEM) observations of a uniaxially deformed PE sample, Kilian et al. (Kilian & Pietralla, 1978) have identified the presence of stacks of several lamellae running parallel and forming clusters, the sizes of which are in the range of several hundreds of angstroms. They showed that the elastic behavior for semicrystalline polymers can be explained using a cluster-network model in which the clusters consisting of mosaic blocks are connected by means of tie molecules to the neighboring ones and are considered to operate as junction points. In addition, the microindentation hardness was demonstrated to be governed by the cooperative shearing of the mosaic blocks within the clusters. Separately from Kilian's work, the direct observation of the stacked lamellar units containing three to ten lamellar crystals has been confirmed by Tagawa et al. (Tagawa, 1980) from high-resolution scanning electron micrographs of blown PE films. They emphasized that the stacks of lamellae containing three to ten lamellae act as one unit and do not separate into single lamellae during deformation. A similar structural unit has been already proposed by Peterlin et al. (Peterlin, 1971, 1975) to describe the necking process.

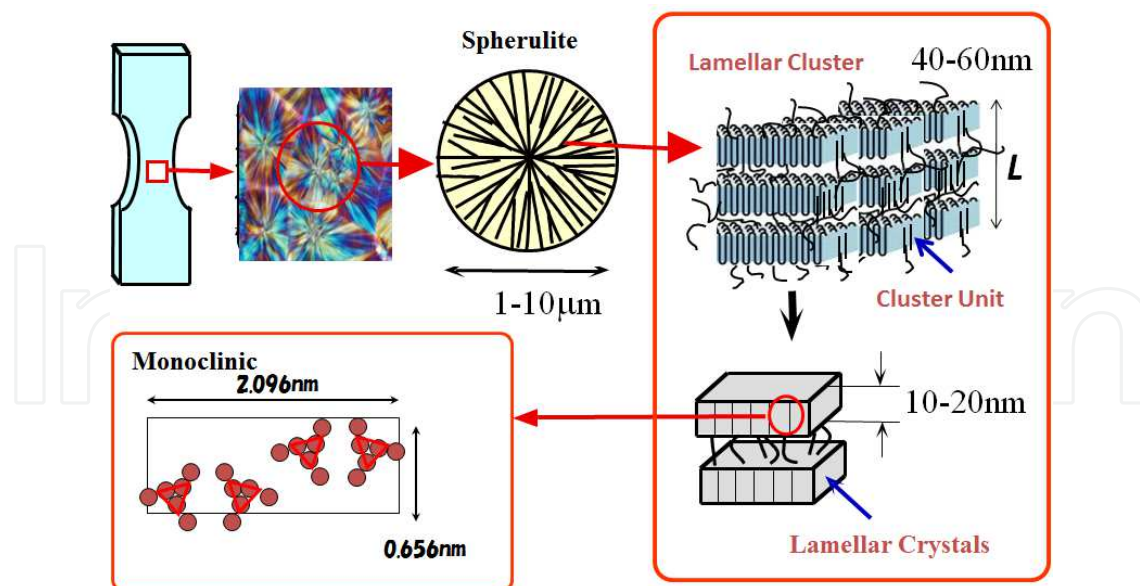


Fig. 1. Supermolecular structure of isotactic polypropylene.

The tensile test is one of the most popular and important mechanical tests. A typical nominal stress-strain curve of semicrystalline solids measured in the temperature range between the glass transition of the amorphous phase and the melting of crystalline phase is illustrated in Figure 2. The stress-strain curve is stepwise and divided into four zones. In the initial strain region, the stress is almost proportional to the applied strain; the deformation proceeds homogeneously and the sample specimen recovers to its original size after the stress is released. Young's modulus can be conventionally estimated from the slope of the line. This region is called the "elastic region". After the initial deformation, the material shows a clear yield point as a maximum point on the nominal stress-strain curve. The maximum point; i.e. yield point is associated with the onset of *temporal* plastic deformation and is referred to as the "failure point". Beyond the yield point, a concave contraction suddenly initiates on the specimen and coalesces into a well-defined neck at which is the onset of the *permanent* plastic deformation. This point is more clearly observed as the second yield point in the case of polyethylene-based materials, but this double yield point seems to be a general feature of semicrystalline polymers as suggested by Séguéla et al. (Séguéla, 1994). Finally, after the necking boundaries have propagated throughout the entire length of the specimen, an upsweep in the stress-strain curve, termed *strain hardening*, occurs, and the stress continues to increase up to the break point. Carothers et al. (Carothers & Hill, 1932) called this phenomenon "cold drawing". In the necking process, the macroscopic morphological transformation from isotropic spherulitic to anisotropic fibril structures takes place accompanied by the destruction and/or rearrangement of parts of the stacked crystalline lamellae. The extension ratio in the neck propagation region is generally defined as the natural draw ratio (Séguéla, 2007).

In general, the transverse strain (perpendicular to the stretching direction under uniaxial elongation), decreases at a constant rate with deformation. The Poisson's ratio is defined as the ratio of the transverse strain to the applied strain. The Poisson's ratio of rubbery materials is in the range of 0.4 to 0.5 (compared to 0.3 for hard materials such as metal or glass). As described above, most semicrystalline polymeric materials, however, show inhomogeneous deformation accompanied with neck formation. The evaluation of the

transient change in Poisson's ratio under a uniaxial extension is essential to characterize the inhomogeneous deformation and the stress-strain relationship. The aim of this chapter is to clarify phenomenologically the relationship between tensile mechanical nonlinearity and geometrical nonlinearity resulting from the transient change in Poisson's ratio in crystalline polymers. For the purpose, we examined the transient Poisson's ratio and tensile properties using a series of typical semicrystalline polymers such as isotactic polypropylene (iPP), high density polyethylene (HDPE), and low density polyethylene (LDPE) samples.

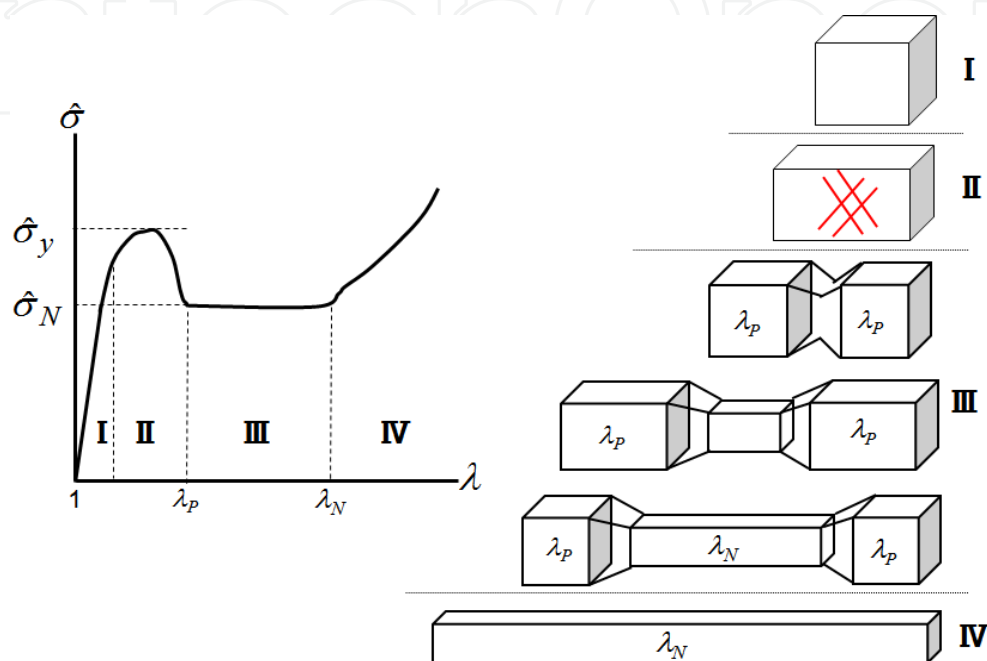


Fig. 2. A typical nominal stress-elongation curve corresponding schematics of deformed specimen during tensile deformation.

## 2. Evaluation of Poisson's ratio

Polymer pellets of isotactic polypropylene (iPP) were melted in a laboratory hot press for 15 min at 230 °C and 10 MPa, and then quenched in ice water (0 °C) or boiling water (100 °C). To control the crystallinity of the iPP sample, we annealed the sample sheets prepared at 0 °C for 2 hr at various temperatures from 40 to 140 °C. Square pillar shaped test specimens were cut out from a 1 mm thick sheet and used for the measurements. Double-edge notched sample specimens with the gauge length of 2 mm were used for the temperature dependence and the dumbbell shaped specimen with gauge length of 5 mm for the elongation speed dependence.

The tensile elongation was performed using a tensile tester which was specially designed with two clamps that move symmetrically with respect to the center point of the specimen. A laser sizer KeyenceLS3934 is mounted on the tensile tester to evaluate the transient thickness of the center of the specimen during tensile deformation. The resolution of the thickness was within  $\pm 2 \mu\text{m}$ . In addition, the three-dimensional change in specimen size during uniaxial elongation was estimated by monitoring successive images of the test specimen with a video camera every 0.5 sec. The experimental setup is shown in Figure 3. The measurements were performed under the following conditions: (1) the nominal strain

rate was changed between 1.25 and 5.00 min<sup>-1</sup>; (2) the temperature was varied within the range of 25 °C to 70 °C; and (3) the degree of crystallinity was changed from 40% to 70% by annealing the iPP sheets quenched at 0 °C in an oven for 2 hr at different temperatures from 40 to 140 °C. Poisson’s ratio values were calculated from the thickness data of each deformed specimen under these conditions. It is noted here that the transient sample dimension in the initial strain region below 0-0.5 sec could not be evaluated.

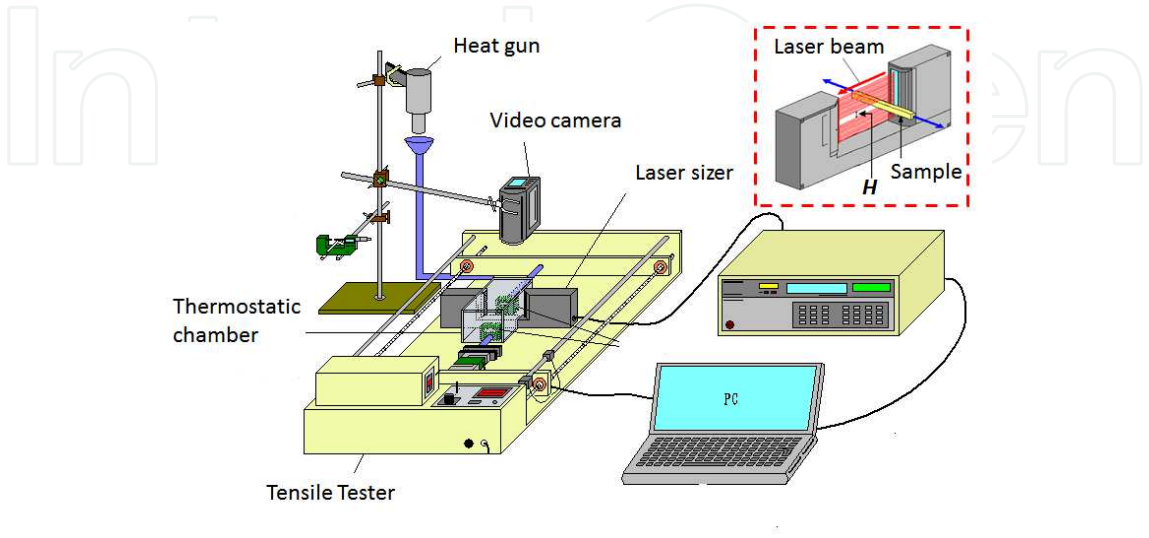


Fig. 3. Experimental setup for simultaneous measurements of the dimensions of the specimen and the external load under a constant elongation speed.

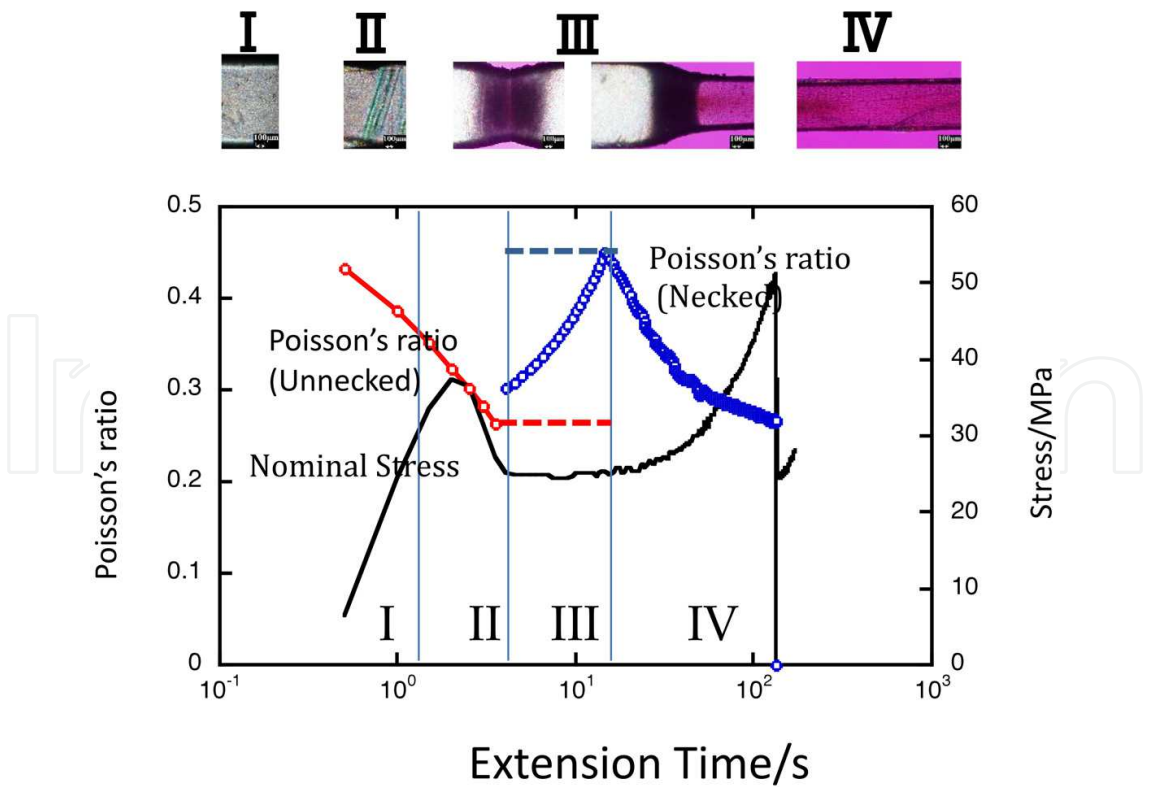


Fig. 4. Poisson’s ratio and nominal stress plotted against the extension time under a tensile elongation at a fixed elongation speed of 20 mm/min.

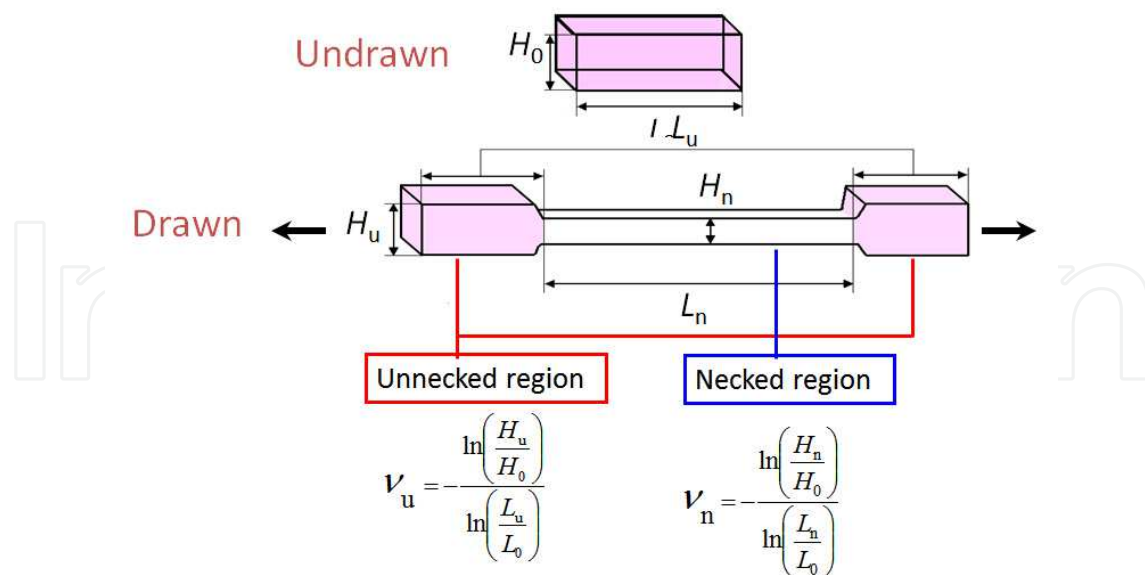


Fig. 5. Poisson's ratio at the necked and unnecked portions of a deformed specimen, where  $v_n$  and  $v_u$  are the Poisson's ratios at the necked (white box) and unnecked portions (red box), respectively.

Figure 4 exemplifies the nominal stress-strain curves and the Poisson's ratio-strain curves for a iPP specimen simultaneously measured at a constant extensional speed (20 mm/min) and room temperature (25 °C). Photographs showing the deformation of the samples are shown above the figure. As seen in this figure, the iPP specimen shows a clear necking phenomenon above the yield point and the strains for both the necking and unnecked regions are almost constant during the neck propagation. The Poisson's ratio values in this figure were estimated from the thickness of the center portion of the deformed specimen under the assumption that the longitudinal strain is given by the extension of the gauge region of the sample specimen. In the pre-yielding region, the value of Poisson's ratio gradually decreases from around 0.5 to zero. The line has been broken at the neck initiation. On the other hand, in the post-yielding region, the Poisson's ratio increases to 0.5 during neck propagation as the necked part grows to encompass the entire specimen. Poisson's ratio has a maximum at the onset of strain-hardening and then monotonically decreases with further increase in applied strain. Since the strains in the unnecked region and the necked region are almost constant, the Poisson's ratio during necking is considered to be an averaged Poisson's ratio.

For the specimens which show clear necking, it is necessary to estimate the Poisson's ratio separately for the necking and unnecked regions. The Poisson's ratios in the unnecked and necked portion were separately estimated from each thickness value for sample specimens with clear necking phenomena, as shown in Figure 5.

### 3. Poisson's ratio under tensile tests

#### 3.1 Elongation speed dependence

To examine the effects of elongation speed, we investigated Poisson's ratio in the range of 5.0 to 20 mm/min (nominal strain rate of 1 to 4 /min) at room temperature, 25 °C.



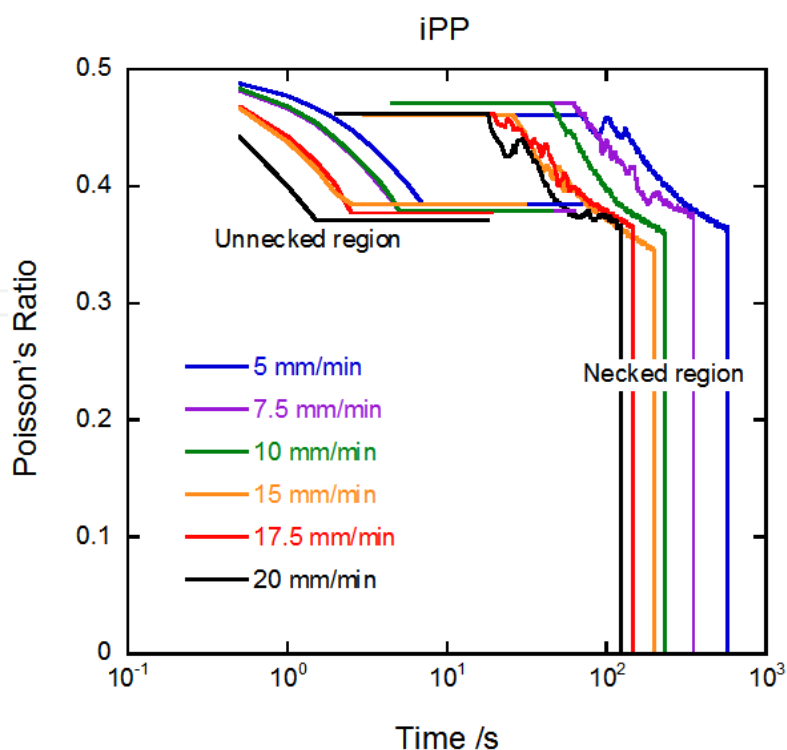


Fig. 6. Elongation speed dependence of Poisson's ratio of iPP at the unnecked and necked regions plotted against elongation time.

Figure 6 shows the Poisson's ratio-elongation time curves in the necked and unnecked regions for iPP. As seen in this figure, in the unnecked region, the value of Poisson's ratio gradually decreases from around 0.5 to around 0.35-0.37 and becomes constant during necking. This indicates that the deformation proceeds mostly through neck propagation after the neck initiation. In the necking region, the Poisson's ratio of the necked portion was almost constant at around 0.46, and the Poisson's ratio started to decrease again after the termination of necking. It is interesting to note that the samples were broken when the Poisson's ratio reached about 0.33, independent of the elongation speed. In addition, it was found that the Poisson's ratio-time curves simply shift to longer times as the elongation speed increases; the curves can be superimposed on the elongation time axis. The stress-time curves can also be superposed. The data in the necked region could be superposed by merely shifting along the logarithmic time axis for the entire elongation range. Figure 7 shows the shift factor of the Poisson's ratio vs elongation time curves at a reference elongation speed of 20 mm/min. There is a linear relationship between the shift factor and the elongation speed. Using this relationship, we can determine the Poisson's ratio-elongation time curves at any elongation speed.

HDPE also showed clear necking. The necking initiation time decreases with increasing elongation speed, similarly to iPP, but the level of Poisson's ratio monotonically decreases with increasing elongation speed, as shown in Figure 8. It is interesting to note that the Poisson's ratio in the necking region is strongly dependent on the elongation speed. In contrast, the Poisson's ratio is relatively insensitive to the elongation speed in the post-necking region, with no clear differences in the Poisson's ratio-elongation time curves observed within experimental error (unlike the behavior observed for iPP). The Poisson's

ratio at the break point was about 0.36 similar to that of iPP, and independent of the elongation speed.

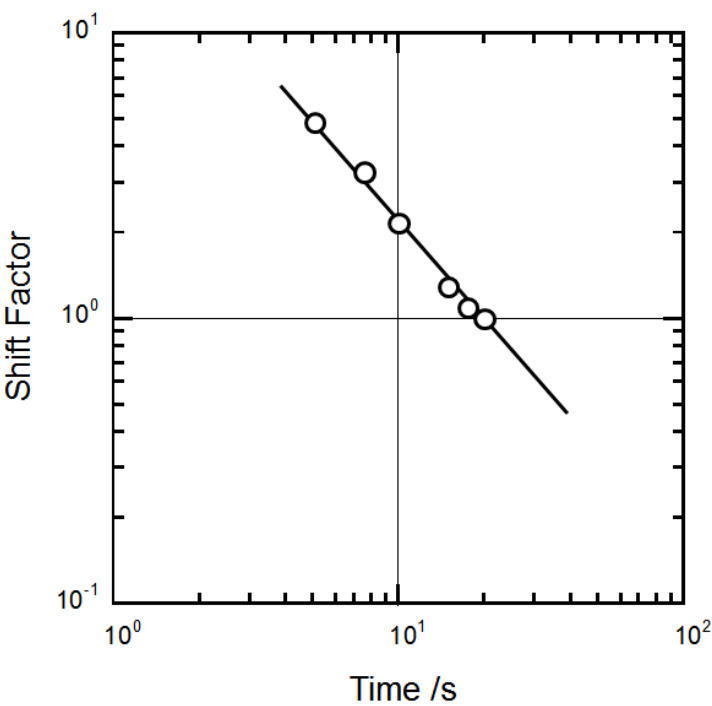


Fig. 7. Shift factor of Poisson’s ratio of iPP for reference elongation speed of 20 mm/min.

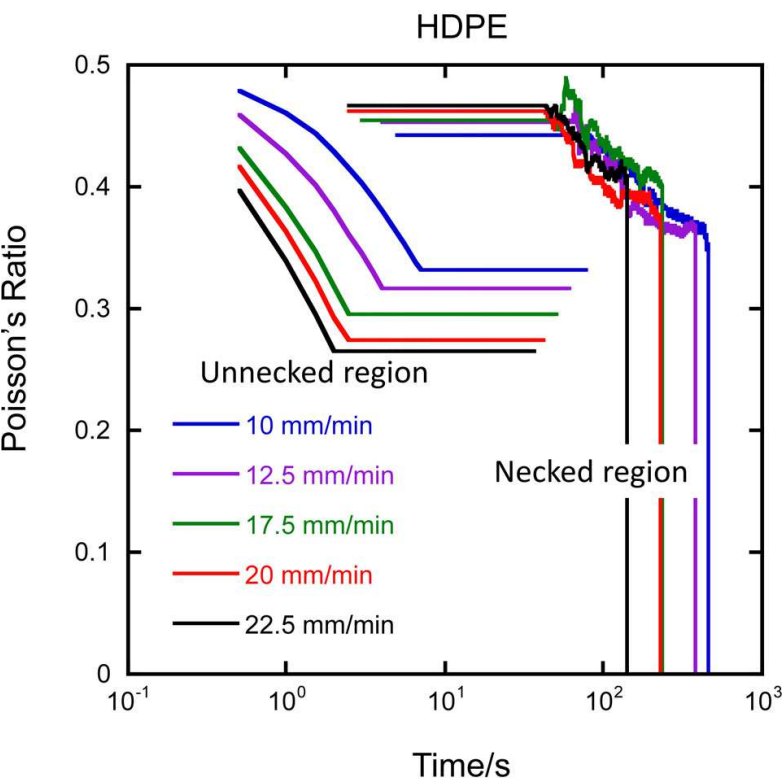


Fig. 8. Elongation speed dependence of Poisson’s ratio of HDPE in the unnecked and necked regions plotted against elongation time.



In the case of LDPE, the necking phenomenon is unclear; no clear necking shoulders in the deformed specimens were observed over the entire experimental range of elongation speeds. Therefore, the Poisson’s ratios in the center of the specimens are plotted against the elongation time. As shown in Figure 9, the minimum point of the Poisson’s ratio corresponds to the initial point of necking, and the maximum point is taken as the natural drawing point. The overall values of Poisson’s ratio are relatively higher than those of HDPE and iPP (which have higher crystallinity), but the Poisson’s ratio markedly decreases with elongation time in the post necking or strain-hardening region similar to HDPE and iPP. It is interesting to note that the maximum point shifts to shorter times as the elongation speed increases and the Poisson’s ratio at break was 0.33-0.36, independent of the elongation speed. Consequently, we can construct a master curve of Poisson’s ratio vs elongation time. Similar to iPP, we have a linear relationship between the shift factor and the elongation time.

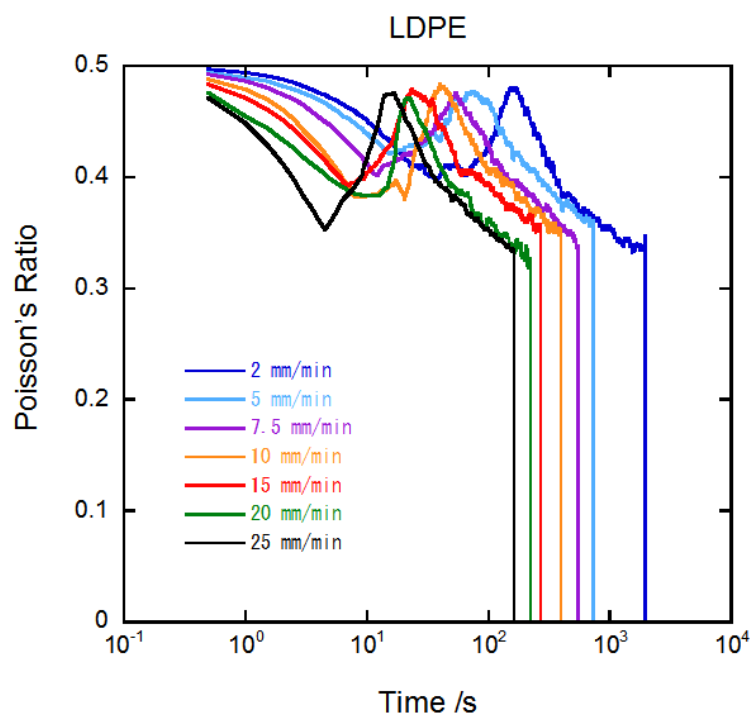


Fig. 9. Elongation speed dependence of Poisson’s ratio of LDPE plotted against elongation time.

3.2 Temperature dependence

To investigate the temperature dependence, we equipped the tensile tester with an environmental chamber where the temperature was controlled within ±0.1 °C. Double-edge-notched specimens with a gauge length of 2mm were employed because of the limited size of the chamber.

Figure 10 shows the temperature dependence of the Poisson’s ratio of iPP measured at a constant elongation speed of 20 mm/min (nominal strain rate of 10 /min). The onset times of necking and strain-hardening were almost independent of temperature and the Poisson’s ratio increases with increasing temperature. The break time is also independent of

temperature. Consequently, the Poisson's ratio-time curves longitudinally shift to higher values with increasing temperature. This indicates that the effect of temperature is not intrinsically coupled with that of elongation speed or nominal strain rate.

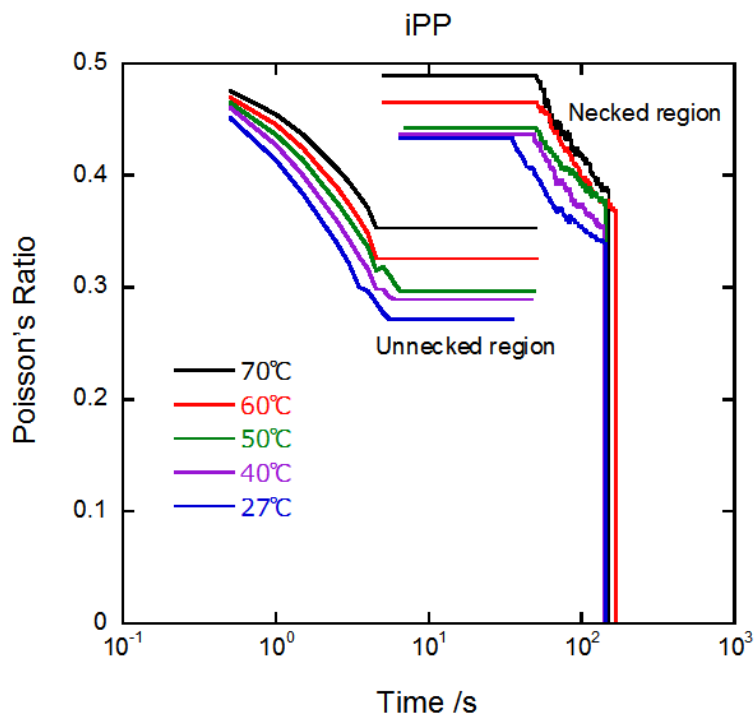


Fig. 10. Temperature dependence of Poisson's ratio of iPP in the unnecked and necked regions plotted against elongation time.

HDPE and LDPE did not reach breaking point owing to their high drawability. As shown in Figure 11, the temperature dependence of Poisson's ratio in HDPE is very similar to that in iPP. The overall level of the Poisson's ratio shifts to higher with increasing temperature, although the Poisson's ratio around the breaking point could not be identified. For LDPE, the minimum (neck initiation) and maximum (neck termination) points of Poisson's ratio appear to be insensitive to the temperature and the overall values approach 0.5 as the temperature increases (see Figure 12).

### 3.3 Crystallinity dependence

Figure 13 shows the crystallinity dependence of Poisson's ratio of iPP at a constant elongation speed of 20 mm/min, initial gauge length of 2 mm (nominal strain rate of 10/min) and 25 °C. In a similar way to the temperature dependence, the onset times of the necking and the strain-hardening as well as the break time were independent of the degree of crystallinity. The Poisson's ratio increases with decreasing crystallinity. This tendency is the same as that shown in the temperature dependence (Figure 10). It is interesting to note that the effects of softening of the materials due to lowering crystallinity are coupled with the effects of softening due to increasing temperature. In the tensile behavior, changing the crystallinity of the materials at a fixed temperature has an equivalent effect on the tensile deformation as changing the temperature for an iPP material with fixed crystallinity. Nitta et al. showed similar effects in the creep behavior of HDPE under fixed true stresses (Nitta &

Maeda, 2010). They showed that time-temperature superposition in creep behavior and crystallinity-time superposition are equivalent for HDPE samples having a wide range of crystallinities. The increase in amorphous phase fraction enhances the overall molecular mobility or extends the experimental timescale, corresponding to the enhancement of molecular mobility due to a rise in temperature.

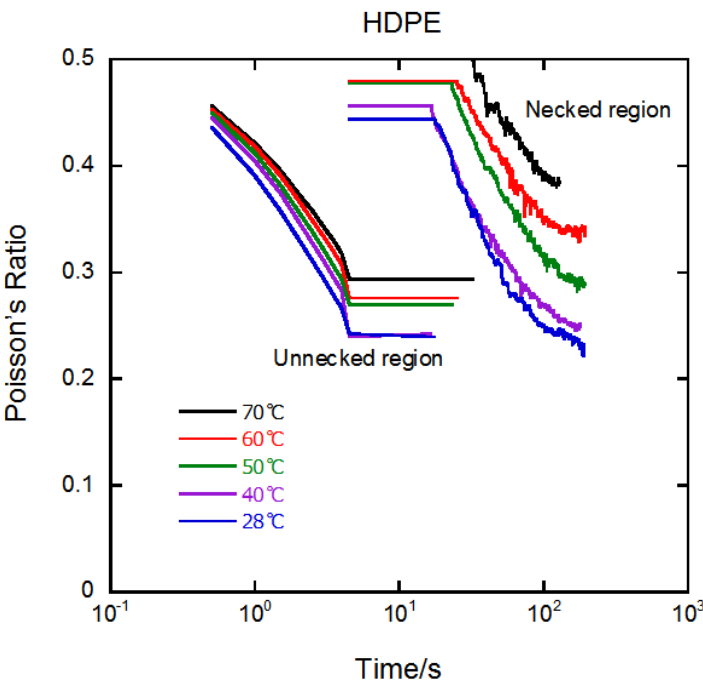


Fig. 11. Temperature dependence of Poisson’s ratio of HDPE at the unnecked and necked regions plotted against elongation time.

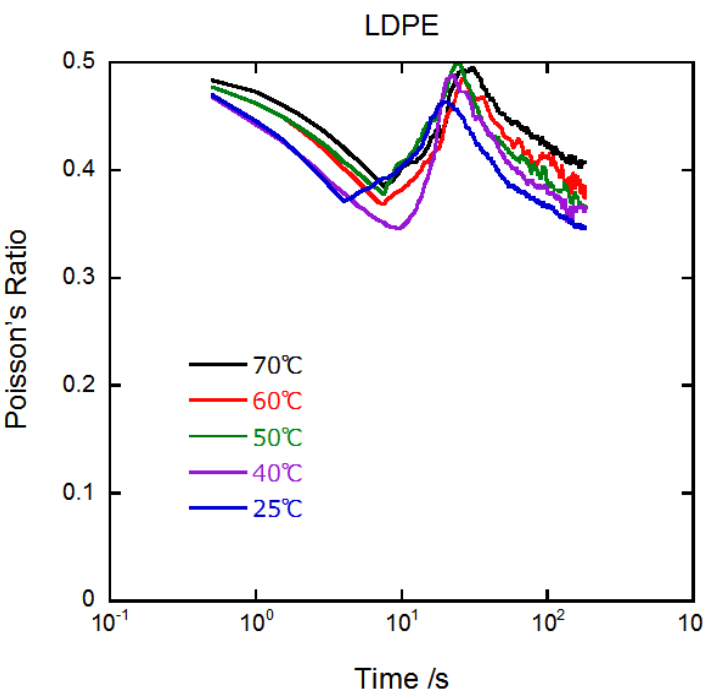


Fig. 12. Temperature dependence of Poisson’s ratio of LDPE plotted against elongation time.

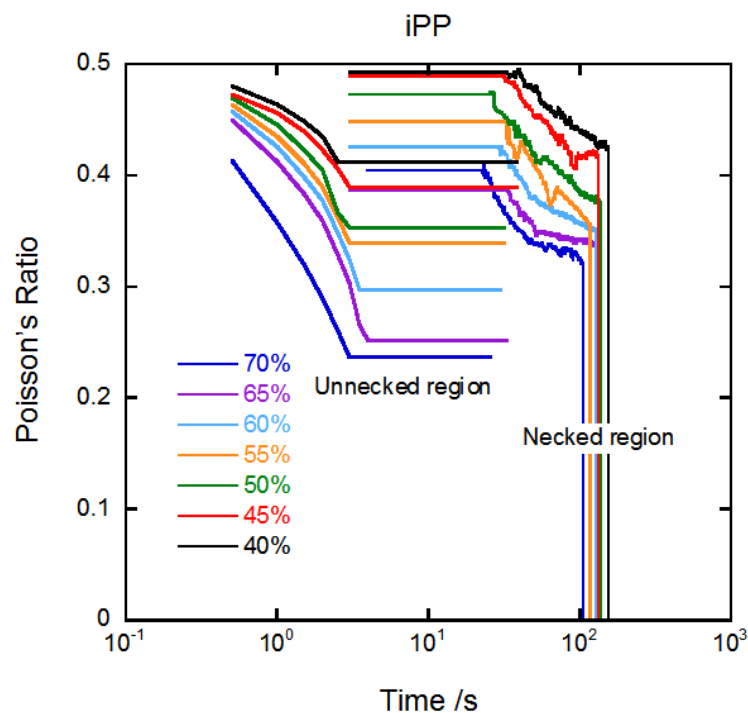


Fig. 13. Crystallinity dependence of Poisson's ratio of iPP in the unnecked and necked regions plotted against elongation time.

## 4. Constitutive relation

### 4.1 Stress-strain relation

Using the Poisson's ratio data, we can convert the nominal load-elongation time data into the true stress-elongation time and true stress-natural (true) strain curves. The true stress values in the necked and unnecked regions were estimated separately from the thickness data of each region. The Hencky strain or true strain values in the necked and unnecked regions were determined separately from the dimension of each region because of the inhomogeneous deformation.

Figures 14 and 15 show the elongation speed dependence of true stress-elongation time and true stress-natural strain curves in the necked region and unnecked region, respectively for iPP and HDPE at different elongational speeds (5-25 mm/min). It is important to note that two stressed states exist in the specimen during necking and the strains in both regions do not proceed during necking. It was found that the stress shows significant nonlinearity; for example, there is a maximum point in the unnecked region, whilst the true stress monotonically increases in a concave upward manner in the necked region. The upsweep in true stress in the necked parts becomes stronger as the elongation speed increases, and the break point was reduced at higher elongation speeds. There are no clear differences in true stress behavior between iPP and HDPE.

The temperature dependences of true stress-elongation time curves of iPP and HDPE are shown in Figures 16 and 17. Again, there are no clear differences in true stress behavior between iPP and HDPE. It is interesting to note that the slope of the initial time region is not sensitive to the temperature and the rise in temperature lowers the yield stress levels at the

maximum. For LDPE, the elongation speed dependence of true stress-time behavior is similar to its temperature dependence, and the overall stress value becomes lower at higher temperatures. It is noted here again that HDPE did not reach a break point in the temperature dependence data.

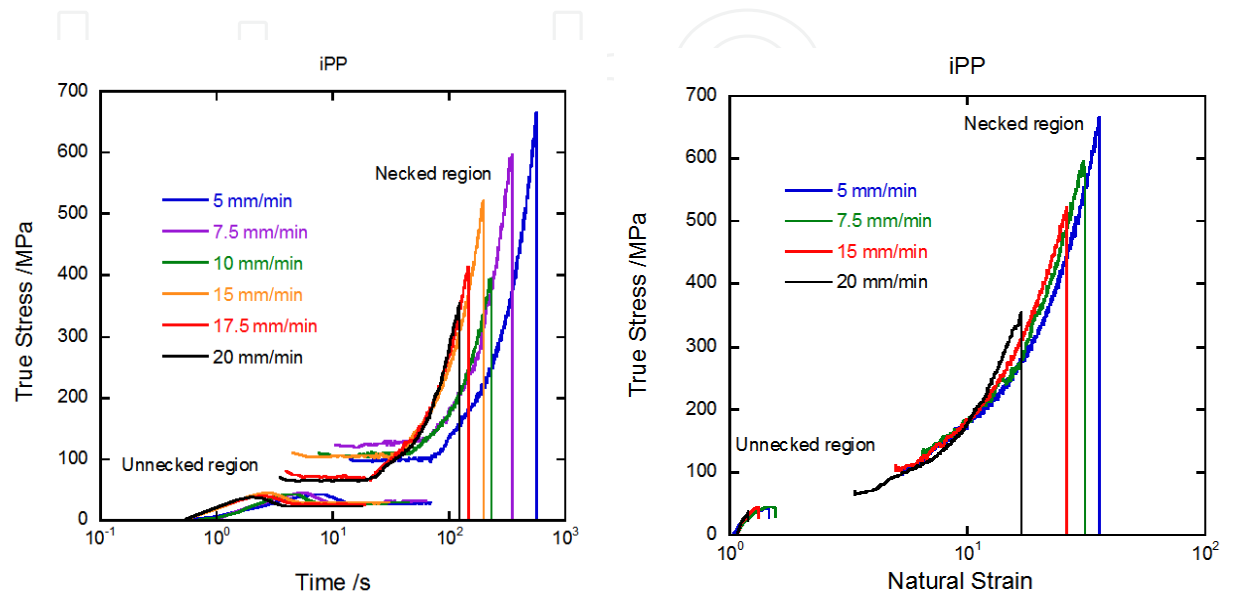


Fig. 14. Elongation speed dependence of true stress-elongation time and true stress- natural strain curves for iPP.

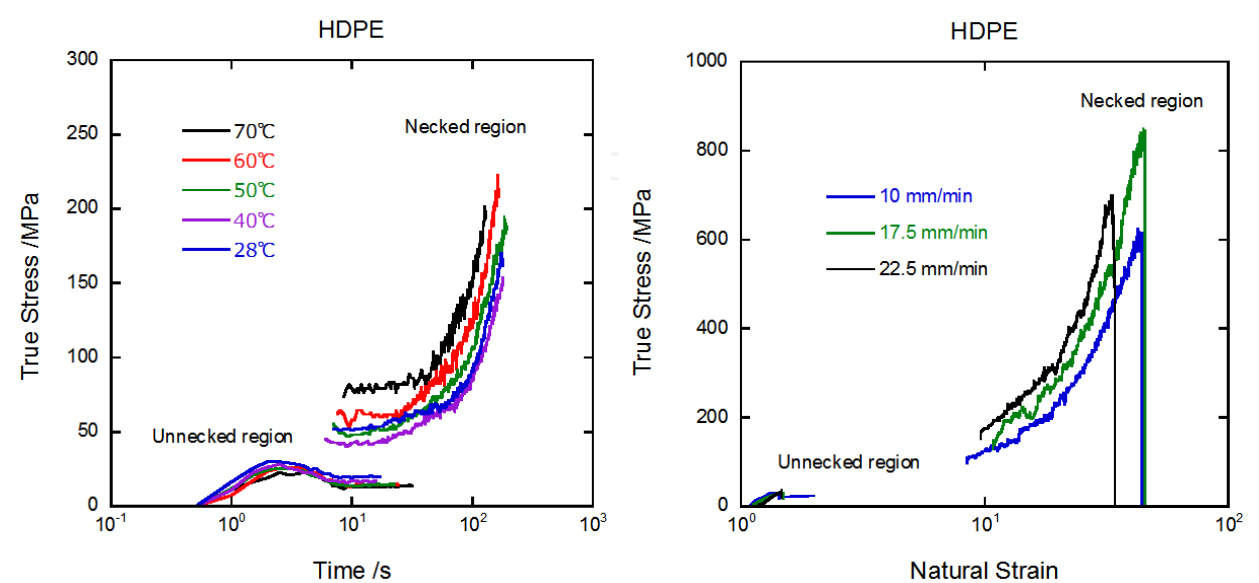


Fig. 15. Elongation speed dependence of true stress-elongation time curves for HDPE.

Figures 18 shows the elongation speed dependence of true stress-elongation time curves for LDPE. Because LDPE shows no clear necking process, the true stress-elongation time curves are not clearly divided into unnecked and necked regions. In the broad necking region, a stepwise increase in the true stress is seen in the curves. The true stress during necking propagation is an average of the true stress values at the maximum Poisson's ratio and the minimum Poisson's ratio.

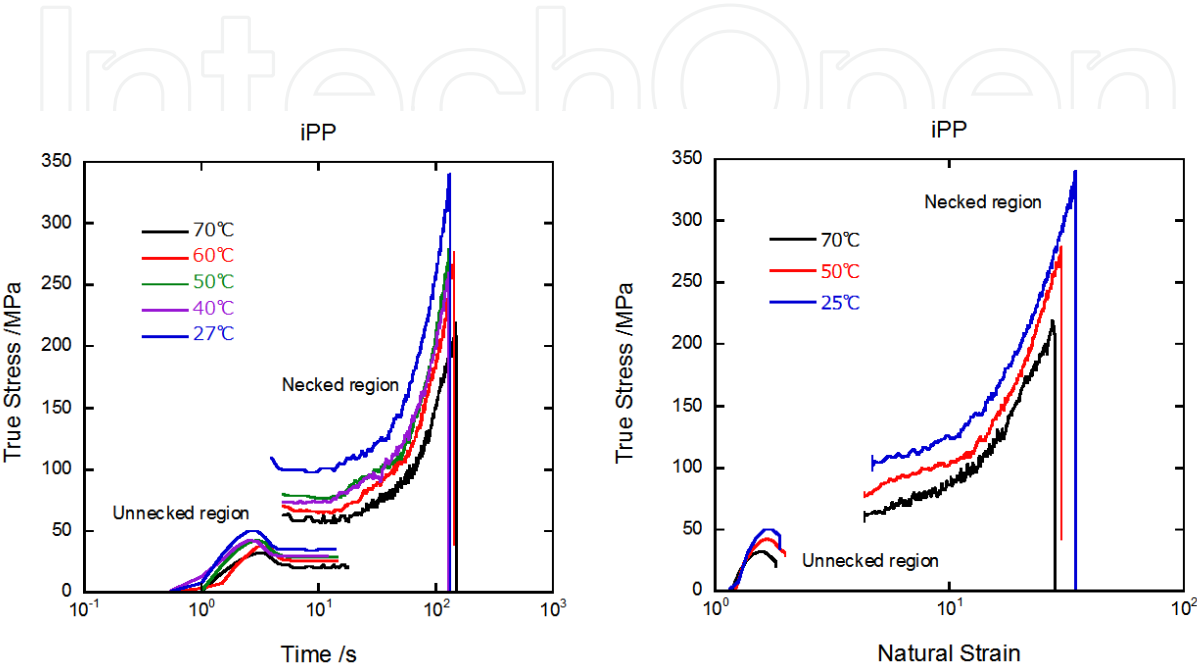


Fig. 16. Temperature dependence of true stress-elongation time and true stress- natural strain curves for iPP.

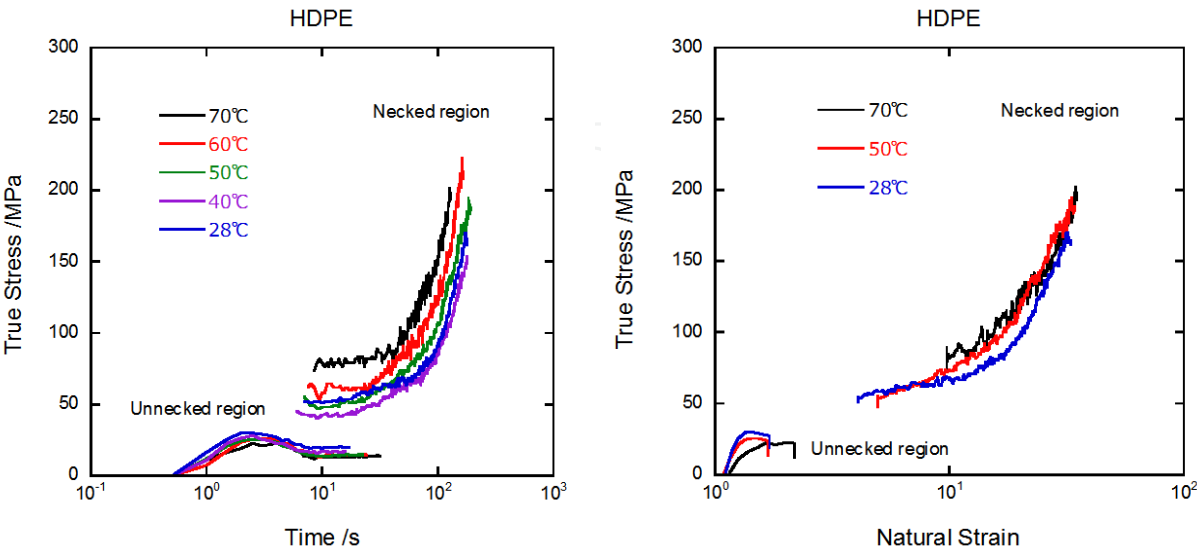


Fig. 17. Temperature dependence of true stress-elongation time and true stress- natural strain curves for HDPE.



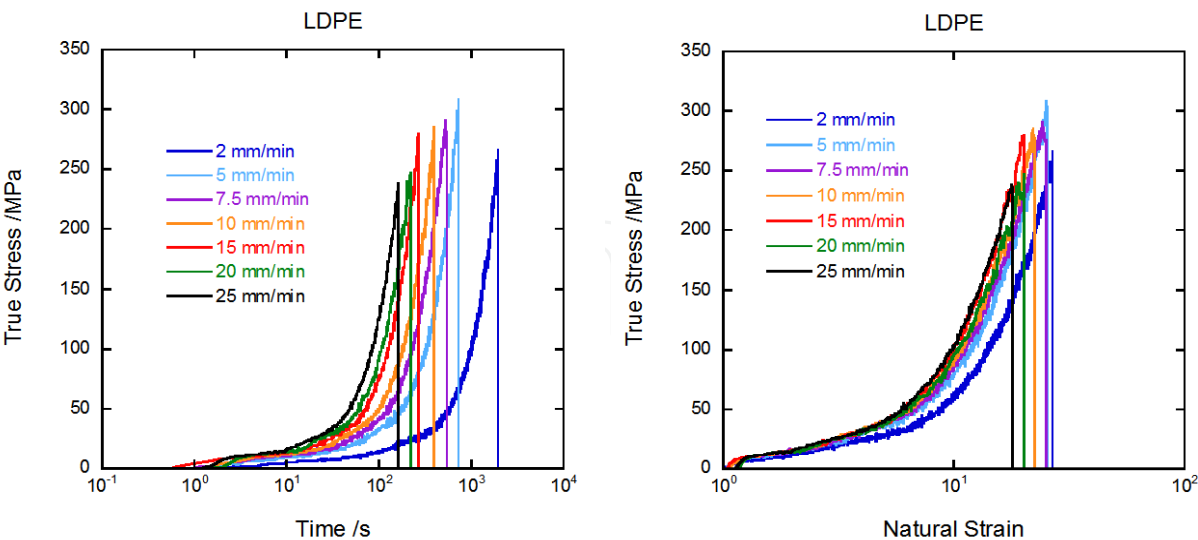


Fig. 18. Elongation speed dependences of true stress-elongation time and true stress-natural strain curves for LDPE.

4.2 Mechanical characteristics

Here we consider the yield stress as a measure of nonlinearity in the unnecked region, i.e. in the pre-necking region, and the strain-hardening coefficient as a measure of nonlinearity in the post-necking region. The yield stress was estimated from the maximum point of each true stress-elongation time curve. The strain-hardening coefficient, defined by Haward et al. (Haward & Thackray, 1968), is given by the modulus based on the true stress reported by the deformation following a neo-Hookean description.

According to Eyring’s kinetic rate theory (Halsey et al., 1945) an equal number of plastic flow units move in the direction of the applied stress  $\sigma_p$  over the potential barrier shifted by the applied mechanical energy  $V^*\sigma_p$ , where  $V^*$  is termed the activation volume but its physical meaning is unclear. When the backward flow is negligible, the frequency  $\nu_p$  of the flow in the forward direction is given by

$$\nu_p = \nu_0 \exp \left[ -\frac{\Delta H - V^* \sigma_p}{RT} \right]$$

(1)

where  $R$  is the gas constant and  $\Delta H$  is the original activation energy for plastic flow. Assuming that the frequency that a flow unit can surmount the potential barrier is related to the rate of change of strain  $\dot{\epsilon}$ , then we have

$$\sigma_p = \frac{\Delta H}{V^*} - \frac{RT}{V^*} \ln \frac{\dot{\epsilon}_0}{2\dot{\epsilon}}$$

(2)

where  $\dot{\epsilon}_0$  is the constant pre-exponential factor which is larger than the conventional  $\dot{\epsilon}$ . Rearranging gives the following relation:

$$\sigma_p = \frac{\Delta H}{V^*} \left( 1 - \frac{T}{T_p} \right) = \gamma_p (T_p - T) \tag{3}$$

where  $T_p = \Delta H / R(\ln \dot{\epsilon}_0 / \dot{\epsilon})^{-1}$  and  $\gamma_p = \Delta H / V^* T_p$ . The yield stress approaches zero as the temperature approaches  $T_p$ , which is in the vicinity of the  $\alpha$ -relaxation temperature, where the crystalline phases start to melt or are in a quasi-molten state (Nitta & Tanaka, 2001). The wide applicability of Eyring model has been demonstrated for a number of polymers (Ward & Sweeney, 2004). Assuming that the plastic stress  $\sigma_p$  corresponds to the true yield stress, the temperature dependence of the yield stress follows Equation (3) as shown in Figure 19.

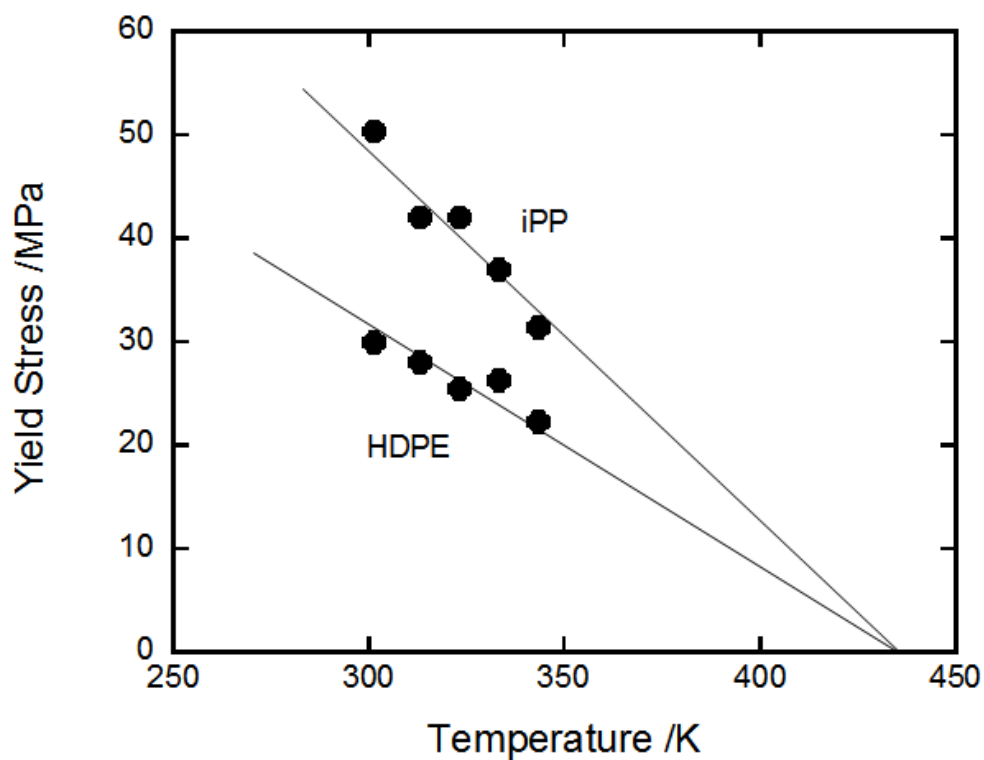


Fig. 19. Temperature dependence of the yield stress of iPP and HDPE.

In addition, Gent et al. presented an interesting concept that the mechanical energy for plastic deformation, yielding and necking corresponds to the thermodynamic melting work (Gent & Madan, 1989). If we accept their idea, Equation (3) can be modified, and  $\Delta H$  can be replaced by  $\chi \Delta H_0$ , where  $\Delta H_0$  may be assumed to be the energy of 100% crystalline material. Then, the yield stress of iPP becomes proportional to the crystallinity in weight fraction  $\chi$ , which was experimentally confirmed as shown in Figure 20.

It has been demonstrated that the tensile stress in the post yielding region, measured over a wide range of elongation speeds and temperatures is given by an additive equation of the plastic component and the network component (G’Sell & Jonas, 1981).

$$\sigma = \sigma_p(\dot{\epsilon}, T) + \sigma_e(\lambda, T) \tag{4}$$

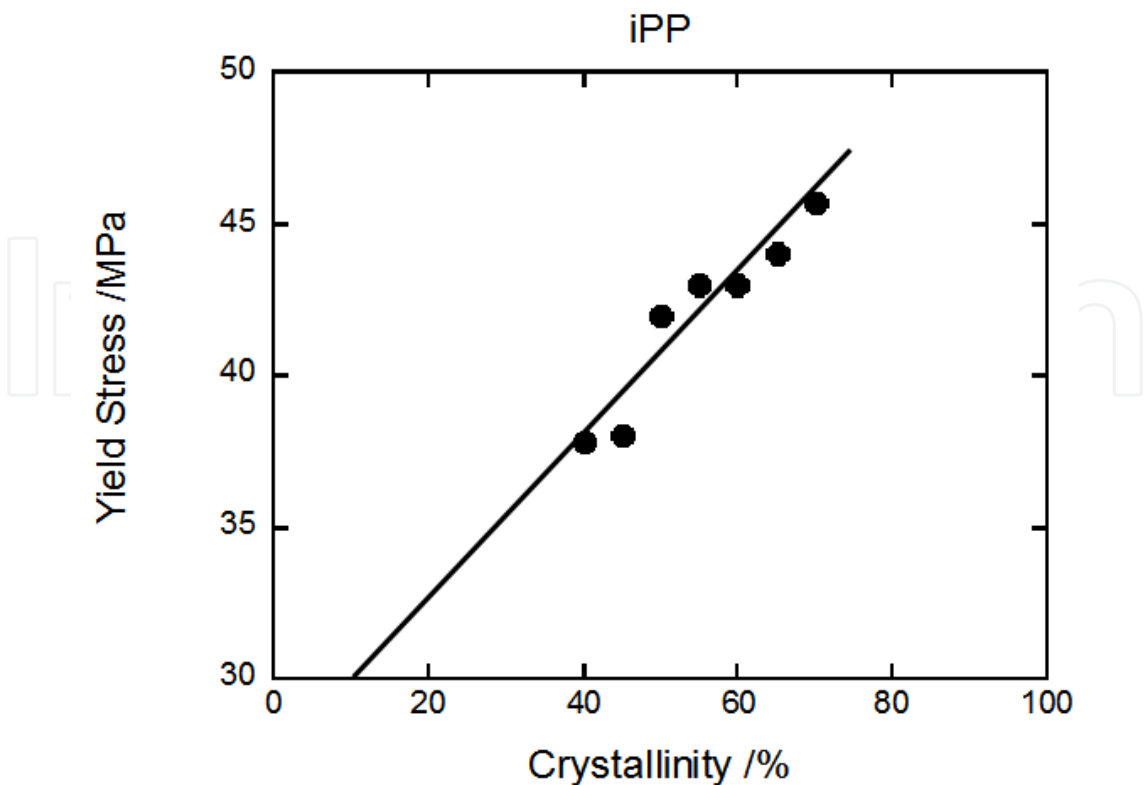


Fig. 20. Crystallinity dependence of the yield stress of iPP.

In the pre-necking region, the yield stress has a positive dependence on elongation speed and a negative dependence on temperature. These empirical characteristics of yielding flow can be expressed by an Eyring rate process.

According to Haward-Thackray theory, the true stress of iPP and HDPE is plotted as a function of the Gaussian strain modified by the transient Poisson’s ratio data. The true stress  $\sigma$  and the modified Gaussian strain  $\varepsilon_G$  were defined using the following equations:

$$\sigma = \hat{\sigma} \lambda^{2\nu} \tag{5}$$

$$\varepsilon_G = \left( \frac{\lambda}{\lambda_{ND}} \right)^{1+2\nu} - 2\nu \frac{\lambda_{ND}}{\lambda} \tag{6}$$

where  $\hat{\sigma}$  is the nominal stress and  $\lambda_{ND}$  is the natural draw ratio (the onset extensional ratio of the strain hardening). When  $\lambda_{ND}=1$  and  $\nu=0.5$ , we have a familiar relation:  $\varepsilon_G = \lambda^2 - 1 / \lambda$ . A Gaussian plot for HDPE gives straight lines, and the slope of the line gives the strain hardening modulus  $G_p$  (see Figure 21). We have an empirical equation as follows:

$$\sigma - \sigma_N = G_p \varepsilon_G \tag{7}$$

where  $\sigma_N$  corresponds to the necking stress in the necked region. The results of iPP showed a deviation of the linearity at the initial Gaussian strains and the  $G_p$  values were estimated from the slope in the higher strain region.

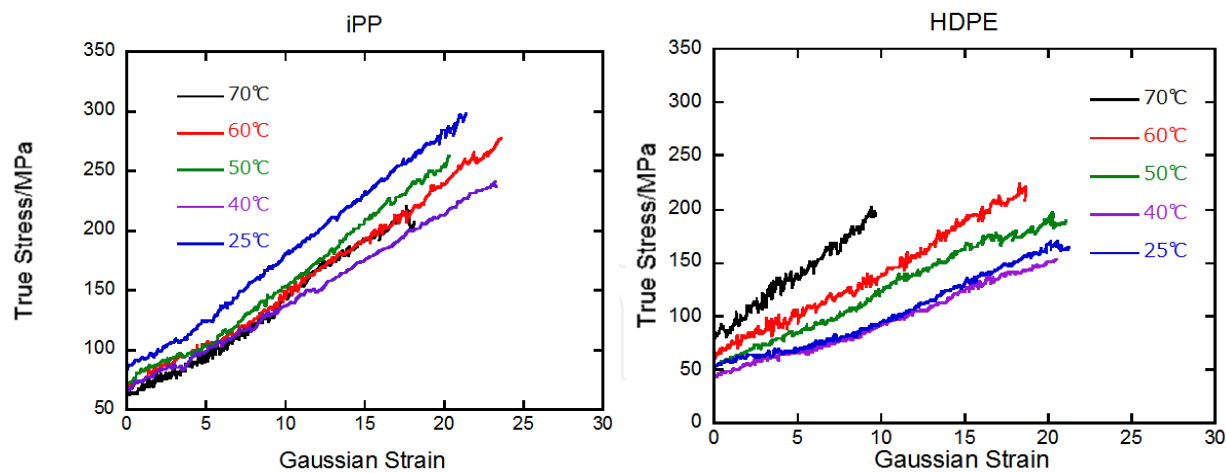


Fig. 21. Gaussian plots for iPP and HDPE

As shown in Figure 22, the  $G_p$  values increase linearly with temperature, empirically given by  $G_p = \gamma_G (T - T_G)$  where  $\gamma_G$  is a positive constant and  $T_G$  is the temperature at  $G_p=0$ , which was almost 0 °C for HDPE. This indicates that entropic network deformation exists within the strain hardening process. It was found that the temperature sensitivity of HDPE is much greater than that of iPP. It should be noted here that the conventional  $G_p$  values, which are estimated from the replotting of the conventional Gaussian strain,  $\lambda^2 - 1 / \lambda$ , decrease with increasing temperature as demonstrated by Haward (Haward, 1993).

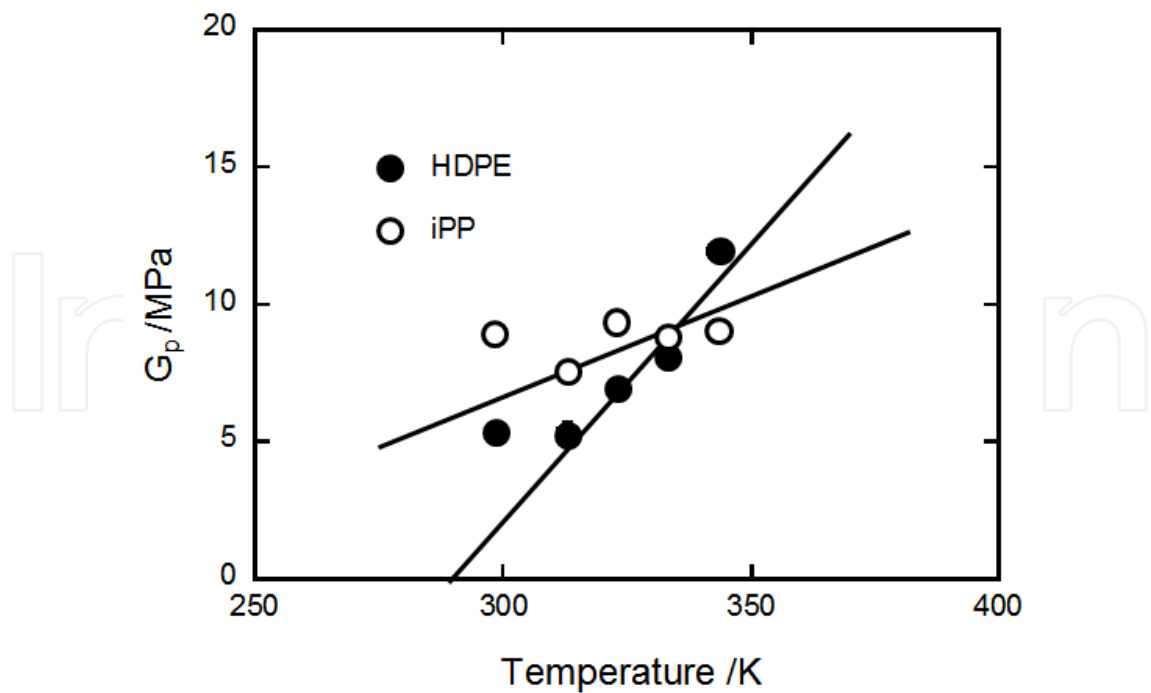


Fig. 22. Temperature dependence of the strain-hardening modulus of iPP and HDPE.

Considering that  $\sigma_N$  is also fitted by an Eyring equation (3) as demonstrated by Nitta et al. (Nitta & Takayanagi, 2006), we have the following simple constitutive equation:

$$\sigma = \gamma_p (T_p - T) + \gamma_G (T - T_G) \varepsilon_G \quad (8)$$

The first term is the plastic component with positive dependence on strain rate and negative dependence on temperature and the second term is associated with an entropic component with positive dependence on temperature.

## 5. Conclusion

Poisson's ratios in crystalline polymers were evaluated precisely from direct measurements of the sample dimensions during deformation over a wide range of extensional speeds, strain rates, temperatures and the degrees of crystallinities of the samples. True stress-strain curves with inhomogeneous deformation could be determined using the transient Poisson's ratio data in the necked portion and unnecked portions. Mechanical nonlinearity is closely related to the nonlinear behavior of Poisson's ratio in each region. We will now describe our conclusions for each region in more detail.

**Elastic region:** In the initial stage of deformation, Poisson's ratio cannot be precisely estimated using our experimental system. This is because the elongation is accelerated until reaching a preset elongation speed just after starting the elongation, and the acceleration causes large experimental errors when estimating precise values of lateral and transverse strains. The Poisson's ratio seems to start at zero, then reach a value consistent with the literature data and remain at that value during deformation up to the yield point.

**Yielding and necking region:** The Poisson's ratio decreases to a minimum value; the Poisson's ratio of the unnecked portion remains at this value during necking. This may be caused by volume expansion due to crazing, cracks, and voids. The Poisson's ratio of the necked part, (i.e. the natural drawn state), becomes nearly 0.5, and the total volume of deformation returns to the volume of the virgin specimen. The values of Poisson's ratio in the unnecked region depend on the extension ratio. As the elongation speed increases, the Poisson's ratio vs elongation curves completely shift to shorter times, resulting in an apparent decrease in Poisson's ratio with increasing elongation speed. On the other hand, a rise in temperature simply enhanced the Poisson's ratio to 0.5.

**In the strain-hardening region:** The true stress linearly increased with the Gaussian strain modified by the transient Poisson's ratio data and the slope of the line, corresponding to the strain-hardening coefficient, showed a positive dependence on temperature. In addition, the true stress-strain relation curves could be described by a linear relationship with the Gaussian strain modified by transient Poisson's ratio data.

## 6. Acknowledgment

This author (K.N) wishes to express his gratitude to the late Professor Motowo Takayanagi for his thoughts and suggestions.

## 7. References

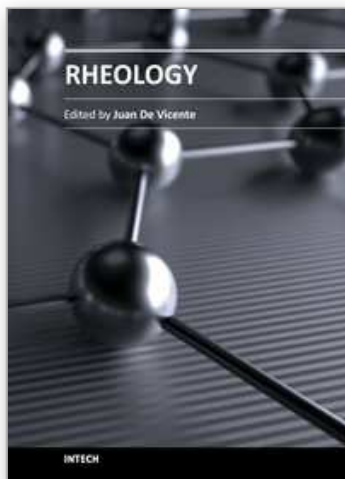
- Balta-Calleja, F.J., Kilian, H.-G., (1985). A novel concept in describing elastic and plastic properties of semicrystalline polymers: polyethylene. *J. Colloid & Polym. Sci.*, 263, 9, 697-707.
- Carothers, W.H., Hill, W.J. *J. Am. Chem. Soc.*, 54, 1579 (1932).
- Ericksen, J. J. (1975). Equilibrium of bars. *J. Elasticity*, 5, 191-201
- G'Sell, C., Jonas, J.J. (1981). Yield and transient effects during the plastic deformation of solid polymers, *J. Mater. Sci.*, 16, 1956-1974
- Halsey, G., White, H.J., Eyring, H. (1945). Mechanical properties of textiles I. *Tex. Res. J.*, 15, 9, 295-311
- Haward, R.N., (1993). Strain hardening of thermoplastics, *Macromolecules*, 26, 22, 5860-5869.
- Heise, B., Kilian, H.-G., Wulff, W. (1980). Deformation and microstructure in uniaxially stretched PE. *Prog. Colloid & Polym. Sci.*, 67, 143-148, ISSN 0340-255X.
- Huchingson, J. W., Neale, K.W. (1983). Neck propagation. *J. Mech. Phys. Solid*, 31, 405-426
- Kilian, H.-G., Pietralla, M. (1978). Anisotropy of thermal diffusivity of uniaxial stretched polyethylenes. *Polymer*, 19, 664-672.
- Kilian, H.-G. (1981). Equation of state of real networks. *Polymer*, 22, 209-217.
- Kilian, H.-G. (1981). A molecular interpretation of the parameters of the van der Waals equation of state for real networks. *Polymer Bull.*, 3, 151-158.
- Kuriyagawa, M., Nitta, K.-H. (2011) Structural explanation on natural draw ratio of metallocene-catalyzed high density polyethylene, *Polymer*, 52, 3469-3477
- Mark, J.E. (1993). *Physical Properties of Polymers* (3rd), Cambridge Univ., ISBN 0 521 53018 0, Cambridge, UK.
- Nitta, K.-H., and Tanaka, A. Dynamic mechanical properties of metallocene catalyzed linear polyethylenes, 42 (2001), 1219-1226.
- Nitta, K.-H., Takayanagi, M. (2006). Application of catastrophe theory to the neck-initiation of semicrystalline polymers induced by the intercluster links. *Polymer J.* 38, 8, 757-766.
- Nitta, K.-H., Takayanagi, M. (2003). Novel proposal of lamellar clustering process for elucidation of tensile yield behavior of linear polyethylenes. *J. Macromol. Sci.-Phys.* 42, 1, 109-128
- Nitta, K.-H., Maeda, H. (2010). Creep behavior of high density polyethylene under a constant true stress. *Polymer Testing*, 29, 60-65.
- Peterlin A, Meinel G. (1971). Small-angle x-ray diffraction studies of plasticity deformed polyethylene. III Small draw ratios. *Makromol Chem.* 142,1, 227-240
- Peterlin A. (1971). Molecular model of drawing polyethylene and polypropylene. *J. Mater. Sci.*, 6, 490-508
- Peterlin A. (1975). Plastic deformation of polymers with fibrous structure. *Colloid Polym Sci.* 253, 10, 809-823
- Strobl, G.R. (1996). *The Physics of Polymers*, Springer, ISBN 3-540-60768-4, Berlin
- Séguéla, R., Darras, O. (1994). Phenomenological aspects of the double yield of polyethylene and related copolymers under tensile loading, *J. Mater. Sci.*, 29, 5342-5352



- Séguéla, R. (2007). On the natural draw ratio of semi-crystalline polymers: Review of the mechanical, physical and molecular aspects. *Macromol. Mater. Eng.* 292, 235-244
- Tagawa, T.; Ogura, K. (1980), Piled-lamellae structure in polyethylene film and its deformation. *J. Polym. Sci. Polym. Phys.*, 18,5,971-979
- Ward, I.M., Sweeney, J. (2004) *An Introduction to The Mechanical Properties of Solid Polymers*. Wiley, ISBN: 047-149626X, New York.

IntechOpen

IntechOpen



## **Rheology**

Edited by Dr. Juan De Vicente

ISBN 978-953-51-0187-1

Hard cover, 350 pages

**Publisher** InTech

**Published online** 07, March, 2012

**Published in print edition** March, 2012

This book contains a wealth of useful information on current rheology research. By covering a broad variety of rheology-related topics, this e-book is addressed to a wide spectrum of academic and applied researchers and scientists but it could also prove useful to industry specialists. The subject areas include, polymer gels, food rheology, drilling fluids and liquid crystals among others.

### **How to reference**

In order to correctly reference this scholarly work, feel free to copy and paste the following:

Koh-hei Nitta and Masahiro Yamana (2012). Poisson's Ratio and Mechanical Nonlinearity Under Tensile Deformation in Crystalline Polymers, Rheology, Dr. Juan De Vicente (Ed.), ISBN: 978-953-51-0187-1, InTech, Available from: <http://www.intechopen.com/books/rheology/poisson-s-ratio-and-mechanical-nonlinearity-under-tensile-deformation>

**INTECH**  
open science | open minds

### **InTech Europe**

University Campus STeP Ri  
Slavka Krautzeka 83/A  
51000 Rijeka, Croatia  
Phone: +385 (51) 770 447  
Fax: +385 (51) 686 166  
[www.intechopen.com](http://www.intechopen.com)

### **InTech China**

Unit 405, Office Block, Hotel Equatorial Shanghai  
No.65, Yan An Road (West), Shanghai, 200040, China  
中国上海市延安西路65号上海国际贵都大饭店办公楼405单元  
Phone: +86-21-62489820  
Fax: +86-21-62489821

© 2012 The Author(s). Licensee IntechOpen. This is an open access article distributed under the terms of the [Creative Commons Attribution 3.0 License](https://creativecommons.org/licenses/by/3.0/), which permits unrestricted use, distribution, and reproduction in any medium, provided the original work is properly cited.

IntechOpen

IntechOpen